

# Effect of tool pin-tip profiles on material flow and mechanical properties of friction stir welding thick AA7075-T6 alloy joints

Mao Yuqing<sup>1</sup> · Ke Liming<sup>1,2</sup> · Liu Fencheng<sup>2</sup> · Chen Yuhua<sup>2</sup> · Xing Li<sup>2</sup>

Received: 23 February 2016 / Accepted: 9 May 2016 / Published online: 25 May 2016  
© Springer-Verlag London 2016

**Abstract** Five tools with different pin-tip profiles like thread taper, triangular, square, three grooves, and conical platform were designed to friction stir weld 20-mm-thick AA7075 alloy plates. The effects of pin-tip profiles on thermal cycles, material flow, and mechanical properties of the joints were studied. The results show that the temperature greatly decreases from the top to the bottom of the weld, and higher peak temperatures along the thickness are obtained using three grooves tool. Due to poor plastic flow reflected by local transfer behavior of material, thread taper and conical platform tools yield macro cross-sectional level pore defect on advancing side in nugget zone. However, triangular, square, and three grooves tools produce defect-free joints due to improving plastic flow resulted from stronger pulsating action and stirring power, leading to higher transfer displacements of local material. The tensile test results show that the joints fabricated by three grooves tool have better mechanical properties including strength and ductility owing to better material flow. A higher ultimate tensile strength of  $391 \pm 10$  MPa, yield strength of  $310 \pm 12$  MPa, and elongation of 8.3 % are obtained, respectively. This can be attributed to finer grains, greater natural aging response and optimum hardness.

**Keywords** Friction stir welding · Pin-tip profile · Thermal cycles · Material flow · EBSD · Mechanical properties

✉ Ke Liming  
liming\_ke@126.com

<sup>1</sup> State Key Laboratory of Solidification Processing, Northwestern Polytechnical University, Xi'an 710072, People's Republic of China

<sup>2</sup> National Defence Key Discipline Laboratory of Light Alloy Processing Science and Technology, Nanchang Hangkong University, Nanchang 330063, People's Republic of China

## 1 Introduction

With characteristics of higher strength to weight ratio, better fracture toughness, and excellent corrosion resistance, 7xxx series aluminum alloys have a wide variety of applications in various industries such as aircraft, aerospace, and automotive. However, 7xxx alloys are difficult to weld using conventional fusion welding methods which are prone to produce solidification cracks, high volume of porosities, and fusion defects [1–4]. 7075 aluminum alloy, a high-strength alloy based on Al–Zn–Mg–Cu system of 7xxx series alloys, is fit for military and aircraft structural components because it can recover strength due to the natural aging after welding [5]. However, welding issues also limit the wider applications of AA7075.

Friction stir welding (FSW) is a solid-state joining process. It is well suitable for welding aluminum alloys which are typically considered to be unweldable [6, 7]. Briefly, FSW transforms the metal into a plastic state using a special tool that rotates and plunges into the butting surfaces resulting in a welded joint. In the joining process, the metal does not melt and recast, so it will avoid cracking problems associated with solidification of the weld metal [8].

So far, investigations on the microstructure and mechanical properties of FSW joints mainly focused on aluminum alloy sheets [9–12]. There have been relatively little publications on FSW of thick Al alloys, in which lots of welding problems still remain. Avettand Fenoel and Taillard [13] found that the nugget hardness in the bottom of weld severely decreased due to lower temperature in FSWing 19-mm-thick AA2050 plates. Similar results were proven by Canaday et al. [14]. They found that the nugget hardness near the weld root was less than at the midplane or near the crown during FSWing AA7050 plates of 32 mm thick, which indicated that the peak temperature in the root was lower than that in the midplane

and crown. Xu et al. [15] reported that the mechanical properties of the bottom slices significantly degraded in FSWing 14-mm-thick AA2219 plates, and a great temperature gradient was found along the weld thickness. In addition, Srinivasa Rao et al. [16] studied that the FSW joint efficiency for the thick plate was only 53 % for 16-mm welds and 70 % for 10-mm welds as against 80~90 % for 3~6 mm sheets of the same material. Based on the abovementioned results, we conclude that a lower temperature and poorer metal flow in the root of the weld result in the performance deterioration of local slices, accordingly reducing global mechanical properties of the joints for FSWing thick plates. Therefore, how to improve the flowability of plastic material in the local weld will be focused on in this study.

It is well-known that the formation characteristics of FSW joints are influenced by material flow and temperature distribution across the weld which are determined by tool geometries and welding parameters [17–19]. The tool geometry, in particular the pin profile, is a predominant factor in determining the weld geometry, localized heating, and stirring action. Besides, it predominantly governs the flow path of plastic material around the pin and is responsible for homogeneous microstructure as well as uniform joint properties [20]. Thomas et al. [21] declared that Whorl™ and MX Triflute™ tool geometries produced higher heat generation and lower displacement volumes of the softened materials during FSW. Zhang et al. [22] revealed that the tool with three-sided pin profile increased its stirring power and hence promoted the metal flow under the probe end due to higher surface velocity at the probe edge. Meanwhile, Thomas and Nicholas [23] demonstrated that the eccentricity allowed incompressible material to pass around the pin profile due to dynamic orbit with relative eccentricity. Elongovan and Balasubramanian [24] showed that pin profiles with square and triangular flat faces were associated with this eccentricity. In addition, triangular and square pin profiles produced a pulsating stirring action in the flowing material due to flat faces, while there was no such pulsating action in the thread taper pin profile. Dawood et al. [25] studied that FSW of AA6061 alloy by using the triangular pin profile produced better stirring effect, resulting in superior mechanical properties of the joints compared to threaded tapered and square pins, less pulsating action experienced in the NZ, leading to the formation of finer grains. However, Khodaverdizadeh et al. [26] reported that square pin profile caused higher degree of plastic deformation which was beneficial to flow of plastic material due to its higher eccentricity and pulsation effect, leading to higher peak temperature and finer recrystallized grains in FSW of copper joints. Therefore, based on the above guidelines, the aim of the present work is to improve temperature and local plastic flow of the weld metal for enhancing mechanical properties of the joints. For this purpose, five different tool pin-tip profiles, thread taper, triangular, square, three grooves, and conical

platform, are designed to weld thick aluminum alloy plates. The welding thermal cycles, local material flow, and mechanical properties of the joints produced by using these five pin-tip profiles are investigated.

## 2 Experimental procedures

In this study, 20-mm-thick 7075-T6 aluminum alloy-rolled plates were used as base material (BM). The chemical compositions and mechanical properties of BM are illustrated in Table 1. The plates were cut into a required size of 300 mm (length) × 75 mm (width) × 20 mm (thickness) and then joined by FSW perpendicular to the rolling direction. A modified horizontal-type milling machine was used. Five different tool pin-tip profiles with thread taper (tool A), triangular (tool B), square (tool C), three grooves (tool D), and conical platform (tool E) coupled with the same left thread were designed to fabricate the joints. The schematic diagram of tool pin-tip profiles is shown in Fig. 1. The tool handle and shoulder were made of H13 die steel, while the pin material was GH4169 steel. The tool sizes were 14 mm in pin root diameter, 8 mm in the head, 19.5 mm in total length, and 2.5 mm in tip height as well as a concave shoulder of 42 mm in diameter. The thread pitch was 2 mm. Constant tool rotation speed of 300 rpm and welding speed of 47.5 mm/min were applied based on the preliminary trail experiments. Moreover, a spindle tilt angle of 2° and a plunge depth of 0.5 mm were kept consistently during FSW.

Temperature curves within the nugget zone (NZ) were measured by using K-type thermocouples with an outer diameter of 1 mm. The thermocouples were located at the top and the bottom of the weld, respectively. Two temperature transducers (ADAM-4188) were used to magnify the millivoltage signals from the thermocouples. A control computer was employed to collect and process the data information. To accurately measure different temperature fields, the positions of the blind holes with 1.1 mm diameter were designed. Figure 2 shows the arranged positions of blind holes drilled on the cross section of the plate.

The samples for metallographic examination were cut perpendicular to the welding direction, mounted, mechanically ground, polished, and etched using the Keller's reagent (2 ml HF, 3 ml HCl, 5 ml HNO<sub>3</sub>, and 190 ml H<sub>2</sub>O) as per the ASTM standard E407 and examined by optical microscopy (OM). A suitable surface finish for electron backscatter diffraction (EBSD) was prepared by applying a standard grinding and mechanical polishing, and an electrochemical compound polishing with a solution of 8 % perchloric acid alcohol for 15 s at -20 °C with an applied potential of 20 V was conducted. Also, a step size of 0.5 μm was used for data collection. The hardness measurements were conducted on the middle cross sections of the joints applying a 0.1-kg load for

**Table 1** Chemical composition and mechanical properties of 7075-T6 aluminum alloy

Chemical composition (wt%)							Mechanical properties				
Mg	Zn	Cu	Si	Fe	Mn	Cr	Al	$\sigma_b$ (MPa)	$\sigma_{0.2}$ (MPa)	A (%)	Hardness (HV)
2.68	5.81	1.66	0.35	0.61	0.33	0.2	Bal.	535	470	8.7	167

10-s dwell time on a HX-1000 model Vickers hardness tester. The interval between two points was 1.0 mm. The tensile specimens were cut perpendicular to the welding direction into a dog bone shape according to ASTM B557M-10. The dimensions of the tensile specimen are shown in Fig. 3. The tensile tests were carried out at a head cross speed of 1 mm/min using a WDS-100 universal testing machine. The tensile properties of each joint were evaluated using three tensile specimens machined from the same joint. The fracture surfaces of the tensile samples were observed using a TESCAN VEGA II-LMH scanning electron microscope (SEM).

### 3 Results and discussion

#### 3.1 Thermal cycles

Figure 4 shows the effect of pin-tip profiles on the thermal cycles along the thickness of the weld during welding. The thermocouples were placed at the top and root of the plate on the retreating side (RS) 7 mm away from the weld center, as shown in Fig. 2 at points 1 and 2, respectively. The temperature curves and peak temperature are presented in Fig. 4a, b, respectively. It is clear that the peak temperature significantly decreases from the top surface to the bottom surface of the weld. The temperature gradient through the thickness is almost more than 50 °C. A maximum temperature of 477 °C on the RS is recorded at the point 1 close to the top surface. Moreover, the peak temperatures produced by other tools are higher than by tool A. The highest peak temperatures at both the top and bottom of NZ produced by tool D are obtained, which are 477 and 425 °C, respectively, as shown in Fig. 4b, which indicates that the tool D can produce more heat input under the same condition.

During FSW, the material experiences continuous shearing and extruding processes, and the heat input is generated from the frictional heat created between the rotating tool and the

workpieces [7, 24]. On one hand, close to the top surface of the weld, the metal experiences stronger frictional and stirring action of the rotating tool shoulder coupled with the pin, but only a smaller stirring force of the pin-tip acts in the root. On the other hand, the contact area and pressure between the shoulder and the workpiece are larger than those between the pin and workpiece. The linear velocity of the shoulder is higher than the pin due to having a bigger radius. In addition, the heat loss in the root caused by thermal conduction between the backing plate and the bottom surface of the plate is much more than that in the top by the heat convection between the top surface and atmosphere. Similar results were reported in refs. [27] and [28]. Therefore, the temperature obviously decreases along the thickness from the top to the bottom of the weld, and a gradient distribution is shown in Fig. 4.

It is believed that, for the same shoulder, the tool pin has a significant effect on the heat generation during FSW. The heat is generated by friction, and deformation varies with pin profile, which will play a crucial role in the material flow path and the degree of plastic deformation [24, 29–31]. Triangular and square pin-tip profiles can produce eccentricity that is expressed as the ratio of the dynamic volume stirred by the tool to the static volume of the tool. Triangular pin-tip profile producing higher eccentricity allows more incompressible materials to pass around the pin, which is beneficial to improve the flowability of plastic material. Compared with triangular pin profile, square pin-tip profile produces more intense pulsating stirring action for the flowing material due to the associated eccentricity, leading to additional friction heat. However, triangular and square pin-tip profiles reduce the interfacial contact areas of the pin with workpiece, which can slightly reduce heat generation and degree of local deformation during FSW [23–26]. Moreover, conical platform pin-tip profile provides an additional downward extruding force for plastic material, which can promote the flowing of the bottom metal. In contrast, three grooves pin-tip profile has a stronger stirring power and hence improve the localized

**Fig. 1** Schematic diagrams of tool pin-tip profiles: **a** thread taper, **b** triangular, **c** square, **d** three grooves, and **e** conical platform

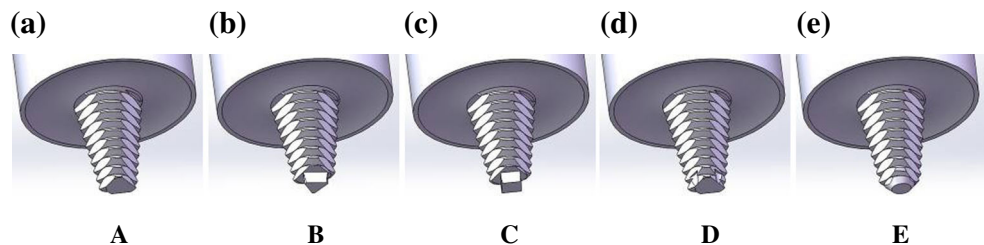
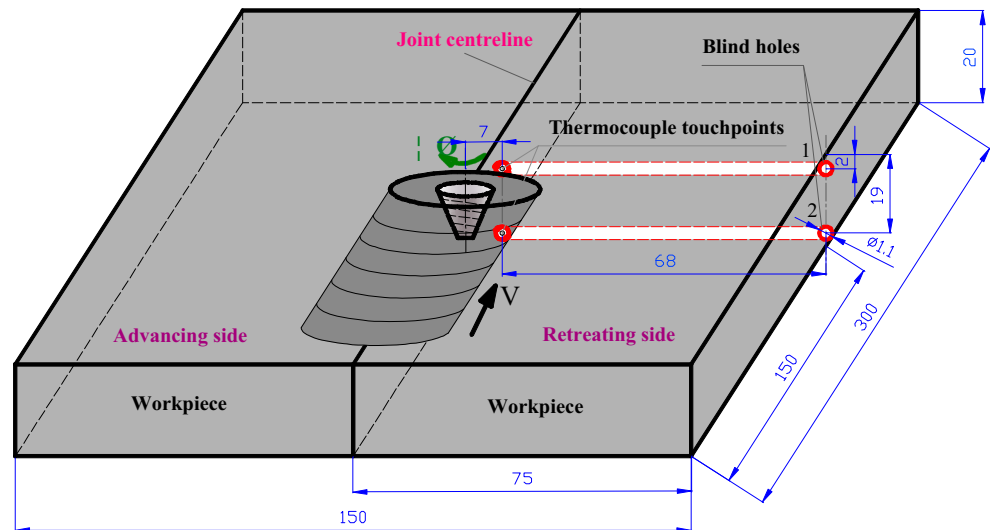


**Fig. 2** Arranged positions of blind holes for measuring temperature during FSW



heating and metal flow under the probe end due to a higher surface velocity at the pin-tip edge, resulting in higher local plastic deformation and more frictional heat to promote the peak temperature in the root of the weld [21, 22]. Hence, the temperature in the bottom welded by tool D is higher in comparison of other tools.

### 3.2 Macrostructure observation

Figure 5 shows the cross section of the welded joints with low magnification; the samples are chosen from the good surface without obvious defects. Seen from the cross sections, defect-free joints can be obtained by using tools B, C, and D. There are no voids, cracks, and other weld defects, as shown in Fig. 5b, c, d, respectively. However, visible voids can be found near the upper middle region of the joints fabricated by tools A and E. Many microvoids are clearly observed (see Fig. 6). The generation of the void indicates that the plastic material insufficiently flows during FSW process due to poor stirring effect. Furthermore, in Fig. 5b, typical FSW onion rings can be seen in NZ of sample B. There is a great difference in size of the area and width of the NZ for different tools in Fig. 5b–d. Compared with other two joints, a bigger area and width of the NZ welded by tool D are obtained. This

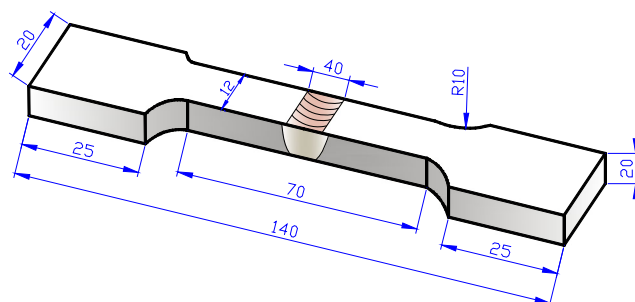


**Fig. 3** All dimensions of the tensile-tested specimens

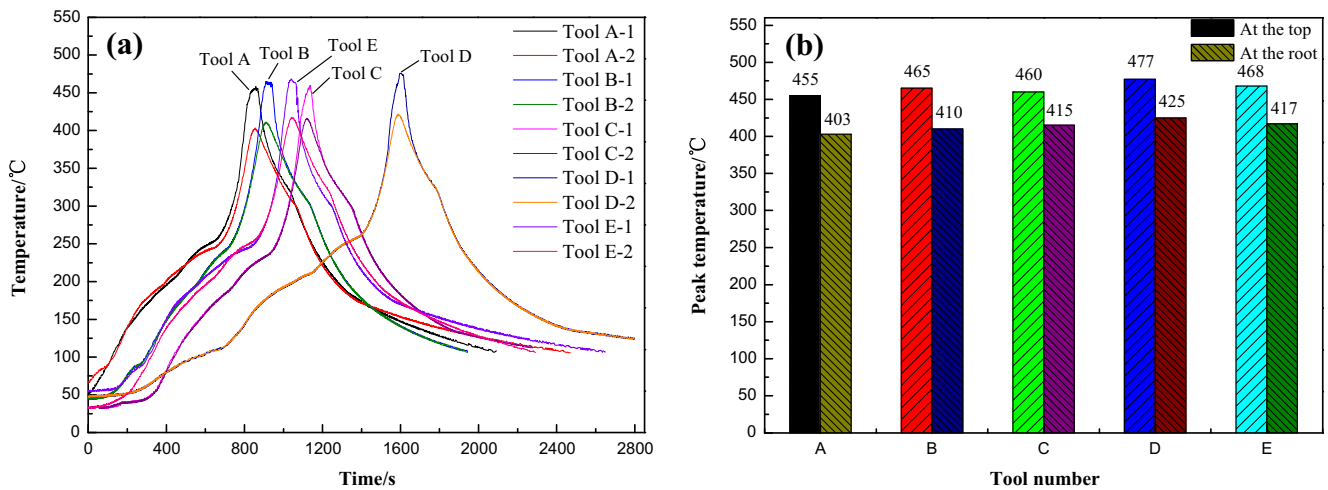
is attributed to the increased heat generation and peak temperature needed for softening the surrounding materials in the NZ (see Fig. 4).

Figure 5 also shows mixing of plastic material in NZ by using tools B, C, and D. The mixing is more uniform than that in other samples. Pin profiles with triangular, square, and three grooves that have higher eccentricity can result in a greater pulsating stirring action [21–23]. The pulsating action leads to more homogenous flowing and mixing of plastic material in NZ which can avoid the pore and tunnel defects. Also, a stronger stirring power with a higher surface velocity at the pin-tip edge can increase the sizes in the area and width of the NZ because of improving the localized heat and material flow. For thread taper pin-tip profile, it is ineffective to produce pulsating stirring action, which causes poor material flow in the weld due to lower temperature and plastic deformation. Conical platform profile exerts an extra downward force to extrude the material transfer horizontally, reducing the upward flow capacity of plastic material, which will form the pore defect on the upper of weld.

### 3.3 Material flow

To further analyze the effect of pin-tip profiles on plastic flow of material in the weld, the local transfer behavior of plastic material is observed (see region C of Fig. 5). Because it is very difficult to get the transfer behavior of material in NZ using the experimental method, the material transfer displacement in thermo-mechanical affected zone (TMAZ) is mainly used to discuss the difference of material transfer behaviors for different pin-tip profiles. Figure 7 shows the local plastic transfer behavior of material on the RS in the middle bottom of the weld at the stable stage of FSW process, in which the transfer direction of plastic material (rolling lines) in the TMAZ is indicated by arrows. It is clear that the material in NZ which





**Fig. 4** Thermal cycles of different welds at the top and the bottom on the retreating side: **a** temperature profiles and **b** peak temperature

contacts the rotating tool moves downwards with the rotation of tool pin, which results in the pileup of material near the bottom of weld. The pileup material in NZ pushes against the material in TMAZ, making the material near rotating tool transfer upwards. In order to intuitively reflect the difference of material transfer behavior influenced by the pin-tip profiles, a maximum upward transfer height ( $\Delta h$ ) is measured, respectively, as shown in Table 2. Obviously, the upward transfer height of material in TMAZ obtained by tool D is the largest compared to other pin-tip profiles, which is about 5.38 mm. The bigger the transfer velocity of material in NZ, the more the pileup material in one unit time near the bottom of weld, which is beneficial to increase the transfer height of material in TMAZ. This indicates that the biggest stirring effect is produced by the three grooves pin-tip profile during FSW process, significantly improving plastic flow of material in the weld.

In general, the joining of the metals at the weld interface is achieved by the frictional heat generated between the tool and the workpieces and material flow. Also, the pin profile has greater effect on the transfer behavior of material. In spite of

the similar heat input range, the different pin profiles alter the material flow, defect formation, and its location [32, 33]. The material below the shoulder is softened to a high extent due to higher temperature. Under the same rotational and welding direction condition, the transport of the softened material starts from the top on the AS. The forward motion of the pin extrudes the plasticized material from the front to the back around the pin. During FSW, the plasticized material adjoining the pin experiences the extruding pressure perpendicular the thread surface and friction force parallel to the thread surface [34]. Under a combined action of those two forces, the plasticized material is driven to flow downwards from the top to the bottom. Since the material cannot be compressed, and the shoulder, the pin, the backing plate, and the undeformed base material create a case like extrusion die, then the material flow path has to be restricted and forced to move upwards at a certain distance after filling out the potential cavity. The schematic diagram is shown in Fig. 8a. In the welding process, the plasticized material is excavated from the AS to RS at the front of the tool and at the rear of the tool pin and flows from the RS to AS to fill the cavity. This is the reason for the defect

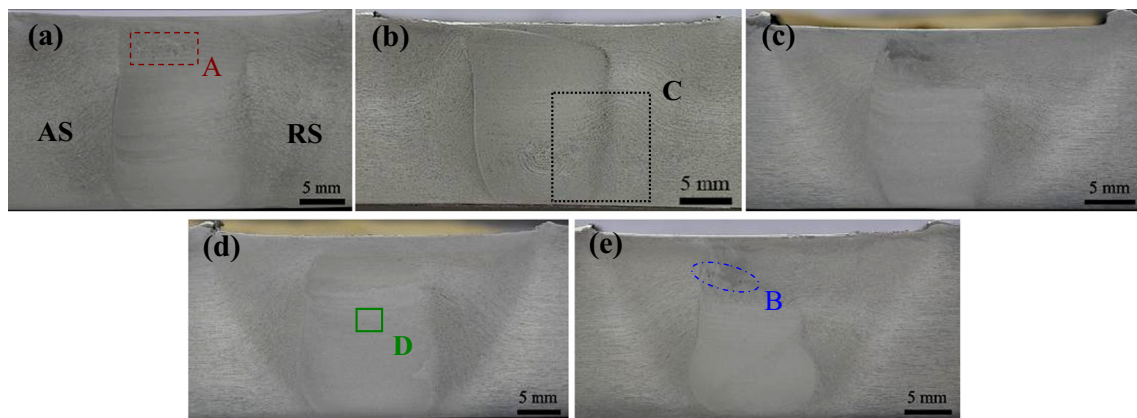
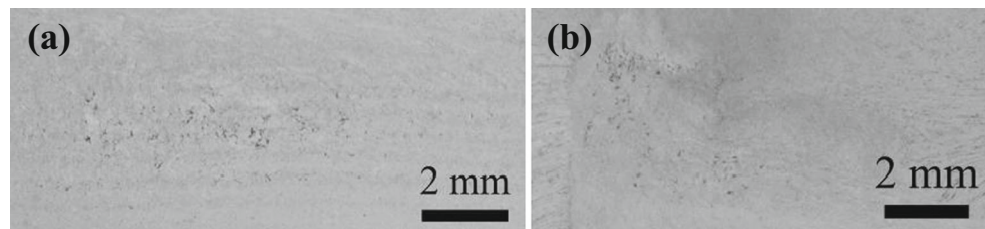


**Fig. 5** Cross sections of the joints made by different tools: **a** tool A, **b** tool B, **c** tool C, **d** tool D, and **e** tool E, respectively

**Fig. 6** Magnifications in the regions A and B in Fig. 5a, e, respectively



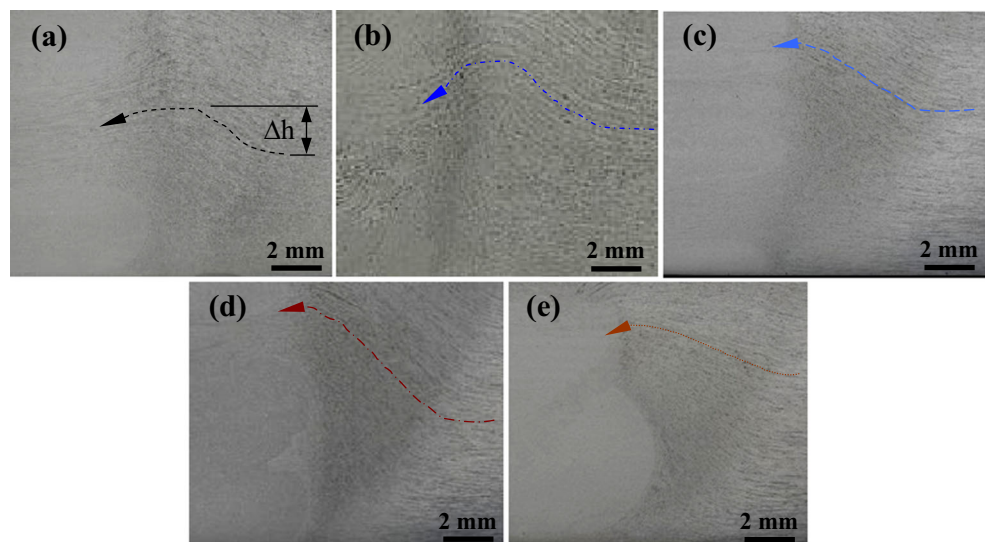
formation on the AS since the thread taper profile and the conical platform profile do not direct the material in such a way to fill the vacancy created during excavation, as shown in Fig. 5a, e.

Moreover, the stirring effect and flow direction of material are greatly influenced by the tool pin profile [17, 20, 31]. For the thread taper pin-tip profile, it cannot produce sufficient stirring effect to drive the plasticized material flow in the abovementioned way, leading to the hole defect. Although the conical platform pin-tip profile can enhance the downward extruding force of the plastic material, it only improves transverse transfer of material in TMAZ while it reduces the upward movement. The triangular and square pin-tip profile can provide an extra pulsating action, which can significantly improve the flowability of the material in the bottom, and then form a defect-free weld. The material in the bottom flows in a spiral vortex way. Meanwhile, the profile with three grooves raises the transfer velocity of plastic material in the root of weld moving upwards from the bottom due to a stronger additional stirring power, which makes the material transfer in a radial diffusion pattern. Various flow modes of plastic material in the weld are presented schematically in Fig. 8 for different pin-tip profiles.

### 3.4 Microstructure characteristics

Figure 7 shows EBSD maps of the grain microstructure in the middle area of the joints (in region D of Fig. 5) welded by different pin-tip profiles. The microstructure in middle nugget zone (MNZ) is characterized by a typical feature of fine equiaxed grains, which is attributed to dynamic recrystallization during FSW. The dynamic recrystallization is a complex nucleation and growth process. The growth is accomplished by the migration of the high-angle grain boundaries (HAGBs). However, different recrystallization mechanisms during FSW are reported [2, 32], including dynamic recovery (DRV), continuous dynamic recrystallization (CDR), discontinuous dynamic recrystallization (DDR), and particle-stimulated nucleation. Relative contributions of the recrystallization mechanisms decide variations of the grain sizes. As is shown in Fig. 7, all MNZs are composed of fine grains with dynamically recrystallized microstructures. However, it is obvious that there is a difference in the grain sizes estimated by EBSD, which are  $11.8 \pm 0.5$ ,  $6.8 \pm 0.3$ ,  $4.7 \pm 0.21$ ,  $2.1 \pm 0.1$ , and  $4.5 \pm 0.19$   $\mu\text{m}$  for MNZs obtained by tool A, tool B, tool C, tool D, and tool E, respectively. The grains are obviously refined in different degrees compared to those in the FSW joints welded

**Fig. 7** Local magnifications of material transfer in the weld bottom on the retreating side obtained by **a** tool A, **b** tool B, **c** tool C, **d** tool D, and **e** tool E, respectively

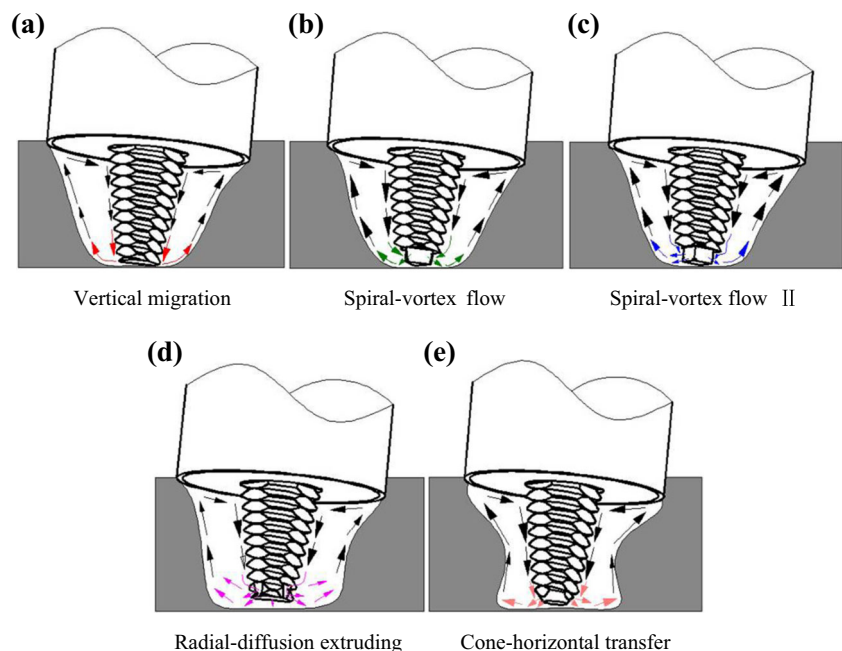


**Table 2** Upward transfer height of material in the bottom of the weld

Tool number	Maximum $\Delta h$ (mm)
A	2.15
B	2.92
C	3.23
D	5.38
E	2.3

using tool A. The grain size obtained by tool D (three grooves pin-tip profile) is the smallest.

It is well known that the pin profile plays a critical role in controlling the flowability and plasticized degree of metals in the weld, which decide the variations in grain sizes [24–26, 29]. For the joint produced by tool A, the microstructures in MNZ are coarse due to poor material flow and low temperature in the weld resulting from a weak stirring force of tool pin in Fig. 9a. Triangular and square pin profiles can produce intense pulsating stirring action due to associated eccentricity, which can generate additional friction heat and higher plastic deformation. It is prone to promote dynamic recrystallization in NZ to some degree, and the grains are smaller shown in Fig. 9b, c. For conical platform pin-tip profile, the microstructure in Fig. 9e is refined attributing to additional downward extruding force. Moreover, three grooves pin profile produces a stronger stirring power and hence promotes the temperature and metal flow in the weld due to a higher surface velocity at the probe edge, leading to the smallest recrystallized grains in MNZ in Fig. 9d.

**Fig. 8** Schematic diagram of flow models of plastic material in the root for different welds

### 3.5 Mechanical properties

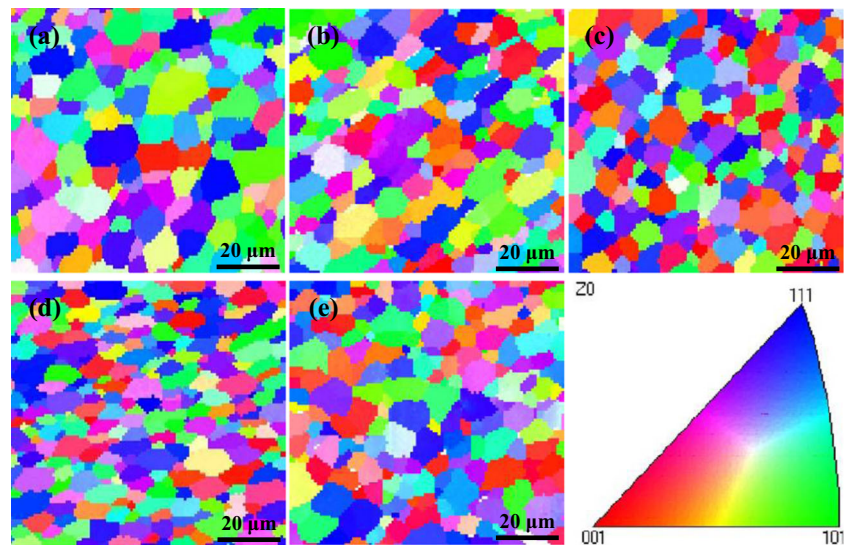
#### 3.5.1 Microhardness

Figure 10 shows the hardness profiles along the mid-thickness of the FSW joints fabricated by different pin-tip profiles. The 7075-T6 alloy exhibits the hardness values in a range of 165–170 HV. It is clear that a typical characteristic with the W-shape is observed along the cross section of the joint, as shown in Fig. 10b. For tool A, the hardness gradually drops before reaching a minimum of 83 HV between the TMAZ and the heat-affected zone (HAZ) and rises slightly to an average level of 117 HV within the center MNZ. With using tool D, the hardness increases rapidly to 143 HV after reaching a larger minimum value of 99 HV. These indicate that W-shaped hardness profiles are obtained along the cross section.

As the hardness profiles can correspond accurately to microstructure evolution, they are used to estimate the property variations of FSW joints of high-strength aluminum alloy. It is well known that the hardness softening throughout the cross section is related to the dissolution and coarsening of strengthening phase particles during welding imposed by the thermal cycles and plastic deformation in 7xxx series alloys [10, 16, 31]. On the other hand, coarse elongated grains near the edge of the TMAZ also lead to the decrease in the hardness basing on the Hall–Petch relationship [35]. The hardness within the center MNZ is significantly influenced by further reprecipitation during and after cooling dependent on the peak temperature, which is proved by the differences in the hardness profiles. The W-shaped hardness profiles with some hardness recovery in the center MNZ could be mainly due to



**Fig. 9** EBSD micrographs showing the grain morphologies in the middle of nugget zone welded by **a** tool A, **b** tool B, **c** tool C, **d** tool D, and **e** tool E, respectively



the post-weld natural aging response, where a further precipitation occurs because of remaining the supersaturated solute in the weld after a fast cooling [2, 36, 37]. Therefore, it can be inferred that, by using tool D, increasing the peak temperature and the exposure time can increase the degree of supersaturation remaining, leading to a greater natural aging response. The hardness recovery in the center MNZ is more obvious, reflecting higher hardness values in Fig. 10a.

### 3.5.2 Tensile properties

In order to evaluate the effects of tool pin-tip profiles on mechanical properties, the tensile tests of the welded samples including the nugget zone at the center are conducted. Figure 11a shows the true tensile stress–strain curves of base material (BM) and different joints. Figure 11b reveals the

results of the strength and elongation. Error bars in Fig. 11b indicate the total range of the test results for three samples per joint. It is explicitly seen from Fig. 11b that the ultimate tensile strength ( $\sigma_b$ ), yield strength ( $\sigma_{0.2}$ ), and elongation ( $\delta$ ) of the FSW joints of AA7075-T6 under different conditions are inferior to those of the BM due to thermal history during FSW. Moreover, it is found that a minimum  $\sigma_b$ ,  $\sigma_{0.2}$ , and  $\delta$  of the tensile joints are obtained when tool A is used, which reach to only  $262 \pm 10$  MPa,  $150 \pm 7$  MPa, and 3.7 %, respectively. For the joints produced by tool D, the mechanical properties of the joints improve significantly, and a maximum  $\sigma_b$  of  $391 \pm 10$  MPa,  $\sigma_{0.2}$  of  $310 \pm 12$  MPa, and  $\delta$  of 8.3 % are obtained, respectively.

Experienced with high temperature and different degrees of plastic deformation, the FSW joint is a heterogeneous composite. Its different component parts possess various

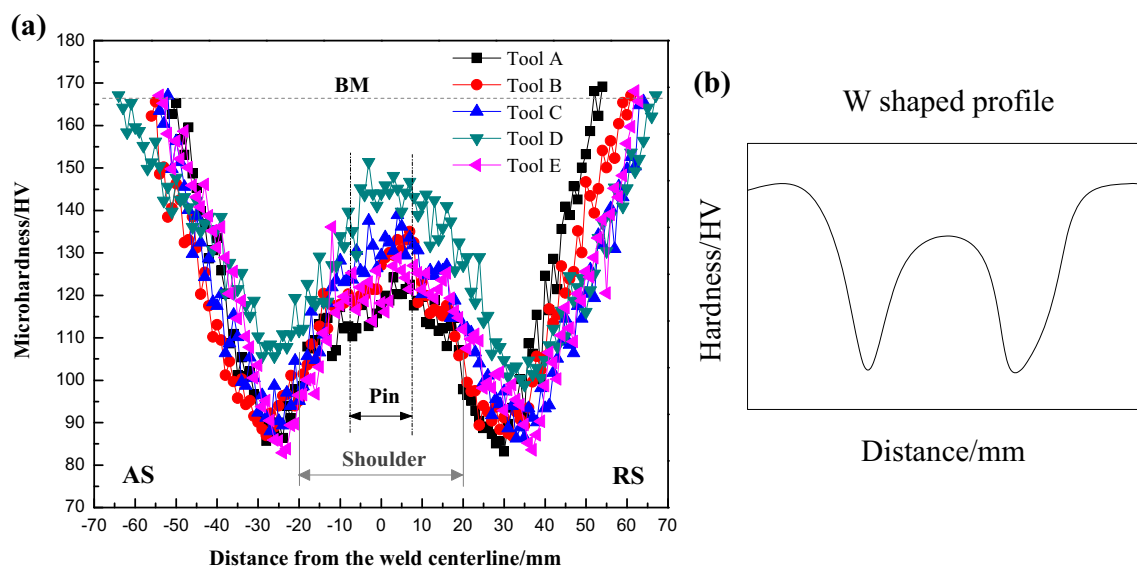


**Fig. 10** Hardness along the mid-thickness of the joints using different tools: **a** microhardness profiles and **b** schematic of W-shaped profile



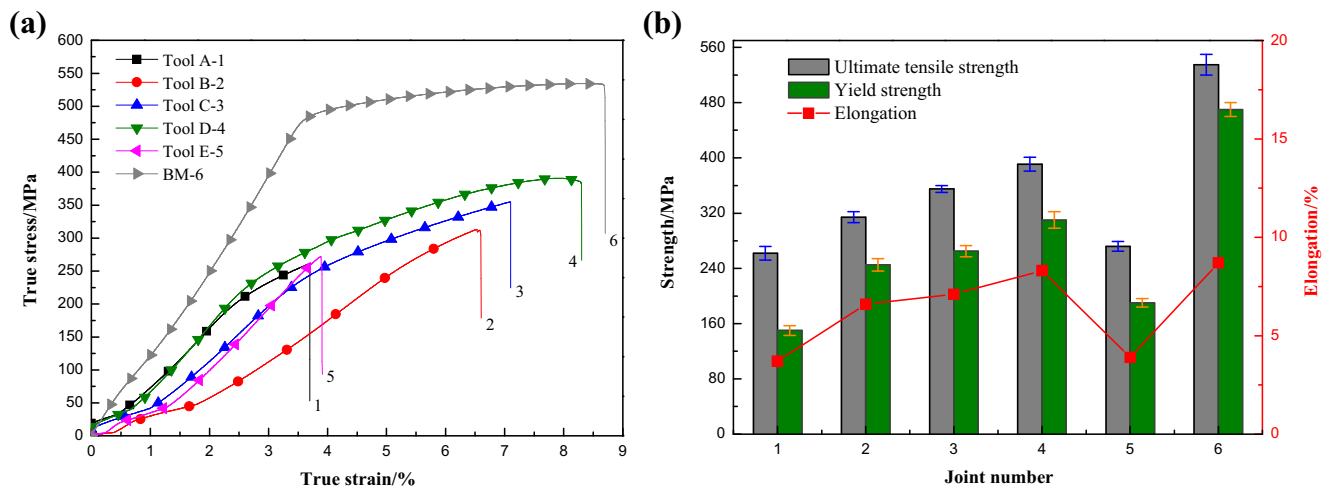


**Fig. 11** Tensile properties of the joints and BM: **a** stress–strain curves and **b** strength and elongation

mechanical properties. The softening region is the weakest and susceptible to the stress concentration during tensile loading. This is the reason why the strength and elongation of the FSW joints are much lower than those of the BM. Additionally, lots of microvoids are found on the cross sections of the joints welded by tool A and tool E due to insufficient plastic flow which can severely degrade the mechanical properties. For these joints produced by tool D, the results exhibit better strengths with an increase in the elongation, which owes to more forceful stirring power of the pin, resulting in a better flowability of plasticized material and high peak temperature. The super strength–ductility synergy could be attributed to (1) finer grains, (2) greater natural aging response, and (3) optimum hardness.

### 3.5.3 Fracture location and morphology

Table 3 presents the fracture locations of FSW joints obtained by different pin-tip profiles. It is clear that, on a macroscopic scale, most macrofracture surfaces of the tensile-tested joints present 45° shear fracture along the tensile axis. Two main fracture modes can be recognized, defined as mode I and mode II. In Mode I, the fracture occurs near/in the NZ. In mode II, however, the fracture occurs at the HAZ. For mode I, it is the most common one regardless of the welding conditions. In this mode, the crack initiation sites do not relate to any softened regions within the NZ. If the weld macrographs (see Fig. 5) are considered, the initiation sites can coincide well with void defect and bad border of the TMAZ/NZ. When a larger degree of stirring effect is created by tool D, the softest region in the HAZ could be more favorable for the crack initiation, and then, mode II occurs.

Figure 12 shows the typical fracture morphologies of the tensile joints corresponding to abovementioned modes I and II. Figure 12a, e shows a brittle fracture initiating from the micropores in the welds due to insufficient plastic flow,






resulting in bad metallurgical binding. Nonetheless, other joints reveal some trans-granular fracture morphologies along with deep dimples having various sizes and shapes, and thick tear ridges full of microvoids, which indicate that the failure is ductile, as shown in Fig. 12b, c, d, respectively. In addition, it is seen from Fig. 12d that the dimples are deeper, and tearing edges are thicker, which also reflect better mechanical properties of the FSW joints. Sharma et al. [38] reported that coarser strengthening particles which nucleated from the voids were rich in Mg and Zn elements for defect-free welds. However, finer precipitated phase particles stemmed from the microvoids, which nucleated in the ligament between the primary voids due to the dispersoids. Therefore, the mechanical properties of the joints welded by tool D are significantly improved owing to sufficient material flow in this investigation.

## 4 Conclusions

In this study, five different pin-tip profiles were designed for friction stir welding of 20-mm-thick AA7075-T6 alloy plates. The effects of pin-tip profile on temperature distribution, material flow, and mechanical properties of the joints were investigated. The following conclusions are derived.

1. The temperature obviously decreases from the top to the bottom of the weld. The peak temperature gradient through the thickness is more than 50 °C. A higher temperature in the top and the bottom of nugget zone is obtained by using the three grooves pin-tip profile compared to other profiles, which are 477 and 425 °C, respectively.
2. Of the five pin-tip profiles used, the thread taper and conical platform pin-tip profile tools are sensitive to macro-level defects like voids on the advancing side in nugget zone due to poor plastic flow reflected by upward transfer

**Table 3** Effect of tool profile on fracture properties of the FSWed joints

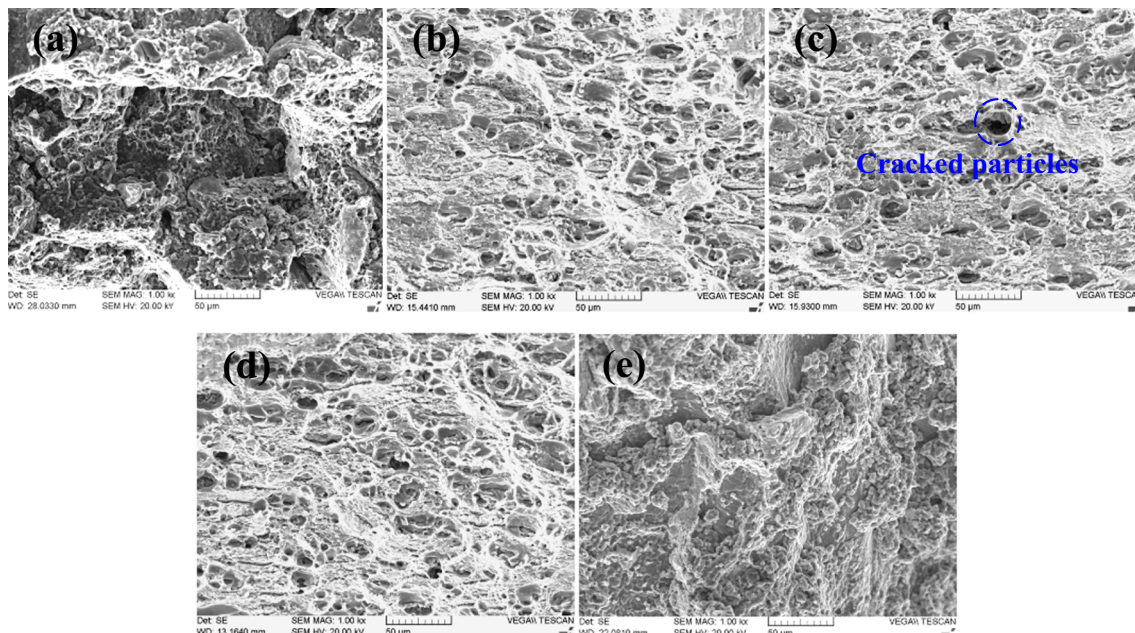
Tool number	Minimum hardness (HV)	Fracture location	Photograph of fractured specimen	
			AS	RS
A	83	NZ		
B	87	NZ		
C	86	NZ		
D	101	HAZ, RS		
E	82	NZ		

behavior of local material, which significantly reduce the tensile properties of the joints.

- The triangular, square, and three grooves pin-tip profile tools yield defect-free cross sections of the joints. The flowability of local plastic material is remarkably improved due to an additional pulsating action or greater

stirring power. The flow paths of materials in the root are mainly presented in spiral vortex flow and radial diffusion extruding patterns, respectively.

- With compared to the triangular and square pin-tip profiles, the joints produced by the three grooves pin-tip profile have superior tensile properties. A higher ultimate

**Fig. 12** Typical fracture surfaces from different joints produced by **a** tool A, **b** tool B, **c** tool C, **d** tool D, and **e** tool E, respectively

tensile strength, yield strength, and elongation are obtained, which are  $391 \pm 10$  MPa,  $310 \pm 12$  MPa, and 8.3 %, respectively. This is attributed to finer grains, greater natural aging response, and optimum hardness.

**Acknowledgments** This work was supported by the National Natural Science Foundation of China (NSFC) (nos. 51265043 and 51265042) and the Landed Plan of Science and Technology in Colleges and Universities of Jiangxi Province (nos. KJLD12074 and 13055).

## References

- Bahemmat P, Haghpanahi M, BesharatiGivi M, Reshad Seighalani K (2012) Study on dissimilar friction stir butt welding of AA7075-O and AA2024-t4 considering the manufacturing limitation. *Int J Adv Manuf Technol* 59(9–12):939–953
- Fuller CB, Mahoney MW, Calabrese M, Micono L (2010) Evolution of microstructure and mechanical properties in naturally aged 7050 and 7075 Al friction stir welds. *Mater Sci Eng A* 527:2233–2240
- Sharma C, Dwivedi DK, Kumar P (2013) Effect of post weld heat treatments on microstructure and mechanical properties of friction stir welded joints of Al-Zn-Mg alloy AA7039. *Mater Des* 43:134–143
- Aissani M, Gachi S, Boubenider F, Benkedda Y (2010) Design and optimization of friction stir welding tool. *Mater Manuf Process* 25(11):1199–1205
- Feng AH, Chen DL, Ma ZY (2010) Microstructure and cyclic deformation behavior of a friction-stir-welded 7075 Al alloy. *Metall Mater Trans A* 41:957–971
- Fu RD, Sun ZQ, Sun RC, Li Y, Liu HJ, Liu L (2011) Improvement of weld temperature distribution and mechanical properties of 7050 aluminum alloy butt joints by submerged friction stir welding. *Mater Des* 32:4825–4831
- Singh R, Sharma C, Dwivedi D, Mehta N, Kumar P (2011) The microstructure and mechanical properties of friction stir welded Al-Zn-Mg alloy in as welded and heat treated conditions. *Mater Des* 32(2):682–687
- Mao YQ, Ke LM, Liu FC, Huang CP, Chen YH, Liu Q (2015) Effect of welding parameters on microstructure and mechanical properties of friction stir welded joints of 2060 aluminum lithium alloy. *Int J Adv Manuf Technol* 81(5):1419–1431
- Hu ZL, Wang XS, Pang Q, Huang F, Qin XP, Hua L (2015) The effect of postprocessing on tensile property and microstructure evolution of friction stir welding aluminum alloy joint. *Mater Charact* 99:180–187
- Zhang F, Su XK, Chen ZY, Nie ZR (2015) Effect of welding parameters on microstructure and mechanical properties of friction stir welded joints of a super high strength Al-Zn-Mg-Cu aluminum alloy. *Mater Des* 67:483–491
- Rodriguez RI, Jordon JB, Allison PG, Rushing T, Garcia L (2015) Microstructure and mechanical properties of dissimilar friction stir welding of 6061-to-7050 aluminum alloys. *Mater Des* 83:60–65
- Mironov S, Masaki K, Sato YS, Kokawa H (2012) Relation between material flow and abnormal grain growth in friction-stir welds. *Scripta Mater* 67:983–986
- Avettand Fenoel M, Taillard R (2015) Heterogeneity of the nugget microstructure in a thick 2050 Al friction-stirred weld. *Metall Mater Trans A* 46A:300–314
- Canaday Clinton T, Moore Matthew A, Tang W, Reynolds AP (2013) Through thickness property variations in a thick plate AA7050 friction stir welded joint. *Mater Sci Eng A* 559:678–682
- Xu WF, Liu JH, Luan GH, Dong CL (2009) Temperature evolution, microstructure and mechanical properties of friction stir welded thick 2219-O aluminum alloy joints. *Mater Des* 30:1886–1893
- Srinivasa Rao T, Madhusudhan Reddy G, Koteswara Rao SR (2015) Microstructure and mechanical properties of friction stir welded AA7075-T651 aluminum alloy thick plates. *Trans Nonferrous Met Soc China* 25:1770–1778
- Nandan R, Deb Roy T, Bhadeshia HKDH (2008) Recent advances in friction stir welding—process, weldment structure and properties. *Progress Mater Sci* 53:980–1023
- Arora A, Debroy T, Bhadeshia HKDH (2011) Back-of-the-envelope calculations in friction stir welding—velocities, peak temperature, torque, and hardness. *Acta Mater* 59(5):2020–2028
- Gratecap F, Racineux G, Marya S (2008) A simple methodology to define conical tool geometry and welding parameters in friction stir welding. *Int J Mater Form* 1:143–158
- Kumar K, Kailas SV (2008) The role of friction stir welding tool on material flow and weld formation. *Mater Sci Eng A* 485:367–374
- Thomas WM, Nicolash ED, Smith SD (2001) Friction stir welding—tool developments. In: Das SK, Kaufman JG, Lienert TJ, editors. *Aluminium 2001 proceedings of the TMS 2001 aluminium automotive and joining session*, TMS; 213–224
- Zhang YN, Cao X, Larose S, Wanjara P (2012) Review of tools for friction stir welding and processing. *Can Metall Quart* 51(3):250–261
- Thomas WM, Nicholas ED (1997) Friction stir welding for the transportation industries. *Mater Des* 18:269–273
- Elangovan K, Balasubramanian V (2008) Influences of tool pin profile and tool shoulder diameter on the formation of friction stir processing zone in AA6061 aluminum alloy. *Mater Des* 29:362–373
- Dawood HI, Mohammed KS, Rahmat A, Uday MB (2015) Effect of small tool pin profiles on microstructures and mechanical properties of 6061 aluminum alloy by friction stir welding. *Trans Nonferrous Met Soc China* 25:2856–2865
- Khodaverdizadeh H, Heidarzadeh A, Saeid T (2013) Effect of tool pin profile on microstructure and mechanical properties of friction stir welded pure copper joints. *Mater Des* 45:265–270
- Xu WF, Liu JH, Zhu HQ, Fu L (2013) Influence of welding parameters and tool pin profile on microstructure and mechanical properties along the thickness in a friction stir welded aluminum alloy. *Mater Des* 47:599–606
- Mao YQ, Ke LM, Liu FC, Chen YH, Xing L (2015) Investigations on temperature distribution, microstructure evolution, and property variations along thickness in friction stir welded joints for thick AA7075-T6 plates. *Int J Adv Manuf Technol*. doi:10.1007/s00170-015-8182-z
- Scialpi A, De Filippis LAC, Cavaliere P (2007) Influence of shoulder geometry on microstructure and mechanical properties of friction stir welded 6082 aluminum alloy. *Mater Des* 28:1124–1129
- Mishra RS, Ma ZY (2005) Friction stir welding and processing. *Mater Sci Eng R* 50:1–78
- Mao YQ, Ke LM, Liu FC, Liu Q, Huang CP, Xing L (2014) Effect of tool pin eccentricity on microstructure and mechanical properties in friction stir welded 7075 aluminum alloy thick plate. *Mater Des* 62:334–343
- Malarvizhi S, Balasubramanian V (2012) Influences of tool shoulder diameter to plate thickness ratio (D/T) on stir zone formation and tensile properties of friction stir welded dissimilar joints of AA6061 aluminum AZ31B magnesium alloys. *Mater Des* 40:453–460
- Elangovan M, Rajendra Boopathy S, Balasubramanian V (2015) Effect of tool pin profile on microstructure and tensile properties of friction stir welded dissimilar AA6061-AA5086 aluminium alloy joints. *Defence Technol* 11:174–184
- Zhang Z, Xiao BL, Wang D, Ma ZY (2011) Effect of alclad layer on material flow and defect formation in friction-stir-welded 2024 aluminum alloy. *Metall Mater Trans A* 42(6):1717–1726

35. Sato YS, Urata M, Kokawa H, Ikeda K (2003) Hall–Petch relationship in friction stir welds of equal channel angular-pressed aluminium alloys. *Mater Sci Eng A* 354:298–305
36. Su JQ, Nelson TW, Mishra R, Mahoney M (2003) Microstructural investigation of friction stir welded 7050-T651 aluminium. *Acta Mater* 51:713–729
37. Khodir SA, Shibayanagi T, Naka M (2006) Microstructure and mechanical properties of friction stir welded AA2024-T3 aluminum alloy. *Mater Trans* 47:185–193
38. Sharma C, Dwivedi DK, Kumar P (2013) Effect of welding parameters on microstructure and mechanical properties of friction stir welded joints of AA7039 aluminum alloy. *Mater Des* 36:379–390